Analysis of EM Properties of High-speed Moving Cone-sphere Target Coated with Plasma Sheath based on Lorentz-FDTD Method

Xian-Min Guo[1], Hai-Yan Li[1], Yong Bo[1,2*], Wei Chen[1], Li-Xia Yang[1], Zhi-Xiang Huang[1], and An-Qi Wang[1]

[1]Information Materials and Intelligent Sensing Laboratory of Anhui Province
Anhui University, Hefei, 230601, China

[2]East China Research Institute of Electronic Engineering
Hefei, 230600, China
*Corresponding author: boyong@ahu.edu.cn

***Abstract* –** The study of the interaction between moving plasma-coated objects and electromagnetic (EM) waves is the essential factor for the EM problems of high-speed targets. In this paper, the physical model of a moving dispersive medium is developed based on the principle of special relativity to study the EM properties of high-speed moving targets coated with plasma sheath. First, the Lorentz transform is used to introduce the incident plane wave into moving frame. Second, based on the proposed EM model, the EM problems are solved in moving frame by the shift-operator (SO) FDTD numerical algorithm. Finally, the EM results are further converted back into the laboratory frame to analyze the scattered properties of high-speed plasma coated objects. The validity of the proposed algorithm is verified by comparison with the reference solution. On this basis, the influence of relativistic effects produced by the motion of the object and the EM properties of the plasma on the scattering fields of high-speed targets are investigated. This work expands the applicability of the FDTD method and provides a theoretical foundation for solving the scattering properties of high-speed plasma-coated complex shape objects through numerical methods.

***Index Terms* –** Electromagnetic (EM) scattering, finite difference time domain (FDTD), moving plasma, relativistic effects.

I. INTRODUCTION

When a high-speed vehicle performs a highly maneuverable cruise mission in the near space, it will generate violent friction with the surrounding atmosphere, which will promote the ionization of the air around the vehicle, resulting in the formation of plasma sheath wrapping around the vehicle [1, 2]. On the one hand, the plasma sheath will seriously interfere with the wireless communication between the target and the detection radar, and will bring irreversible effects on the electromagnetic (EM) transmission, scattering, and imaging characteristics of high-speed moving targets [3–5]. On the other hand, the relativistic effect due to the high-speed motion of the radar target will modulate the EM wave as well. Therefore, the influence of relativistic effects must be considered in the study of EM scattering properties of high-speed moving targets coated with plasma sheaths.

In real application environments, the acquisition of the realistic flow field environment excited around a high-speed target would be time-consuming and expensive [6], which aggravates the difficulty of the research and analysis of the EM problems about high-speed moving targets coated with plasma sheaths. Numerous EM numerical simulation approaches play a crucial role in real-world applications as computer technology advances. The finite-difference time-domain (FDTD) approach can be used to solve EM problems in a wide range of complicated situations with high accuracy and efficiency, and it can also be effectively integrated with other methods [7–9]. Zheng et al. proposed to introduce the Lorentz transformation into the FDTD method for calculating the EM scattering characteristics of a high-speed moving conductor plate [10]. The EM transmission characteristics of a high-speed moving multilayer dielectric plate are further investigated by using the Lorentz-FDTD method [11]. To analyze the transmission characteristics of EM waves obliquely incident into a high-speed moving left-handed metamaterial, the authors establish a connection between the Lorentz transformation with the ADE-FDTD method [12]. The total energy scattering, extinction, and absorption cross section of incident EM waves by a high-speed moving target are analyzed based on the relativistic principles [13–14]. By transforming LFM waves into the moving frame, the 1D range profile of a high-

Submitted On: June 29, 2023
Accepted On: October 22, 2023

https://doi.org/10.13052/2024.ACES.J.390209

speed moving target is researched in [15] based on the Lorentz-FDTD method. The interaction between EM waves and spatiotemporally non-uniform moving plasma plates is revealed in [16]. In [17], absorption characteristics of EM waves by a non-uniform plasma moving at high velocities were investigated by using the Wentzel-Kramers-Brillouin method.

In summary, various numerical methods have been developed and applied to study the EM scattering characteristics of high-speed targets [7–12, 15] and the effect of moving plasma plates on the EM transmission characteristics [16–19]. However, there remains a dearth of studies on the EM properties of high-speed moving complex-shaped targets coated with plasma sheath based on the relativity effect. In this paper, we investigate the influence of relativistic effects and EM parameters of plasma sheath on the scattering characteristics of high-speed targets by using the Lorentz-FDTD method.

In Section II, the EM scattering model of the moving dispersive medium is established, and the procedure for the calculation of the moving dispersive medium by the Lorentz-FDTD method is derived. In Section III, the validity and accuracy of the proposed algorithm is verified. In Section IV, the EM scattering problem from a uniformly moving conical-spherical metal object and that object coated with a plasma has been investigated and analyzed. The conclusion of this research is presented in Section V.

II. RESEARCH METHOD

The fundamental principle of the calculation of a high-speed moving dispersive medium target by the Lorentz-FDTD method can be divided into two steps. First, the dynamic EM scattering problem in the radar frame (denote by K frame) is converted to the motion frame (denote by K' frame), which remains relatively stationary with the moving target according to the principle of relativity. Second, the EM problem is solved by the conventional FDTD method in the K'frame, and then the EM solution is further transformed into the K frame according to the inverse Lorentz transformation. The relationship between the two frames is shown in Fig. 1. Before the solution of the dynamic EM problem for high-speed targets by the conventional FDTD method, the incident plane EM waves and the spatial-temporal separation intervals in both frames need to be converted according to the relativistic principle. The algorithm flow of the Lorentz-FDTD method for calculating the motion dispersion medium is shown in Fig. 2.

A. Physical model of moving plasma

When EM waves propagate in a moving isotropic medium, their frequency will be shifted due to the Doppler effect. Assuming that the angle between the EM wave propagation vector $\vec{k}$ and the object velocity $\vec{v}$ is θ,

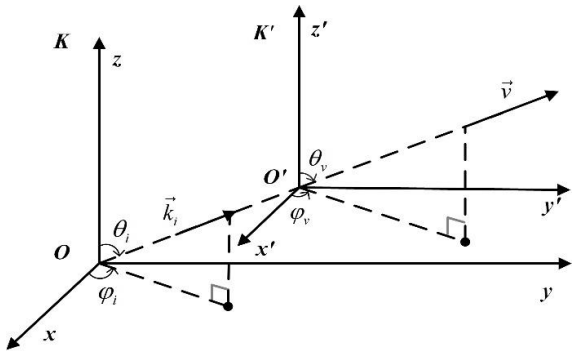

Fig. 1. Sketch of the two coordinate systems.

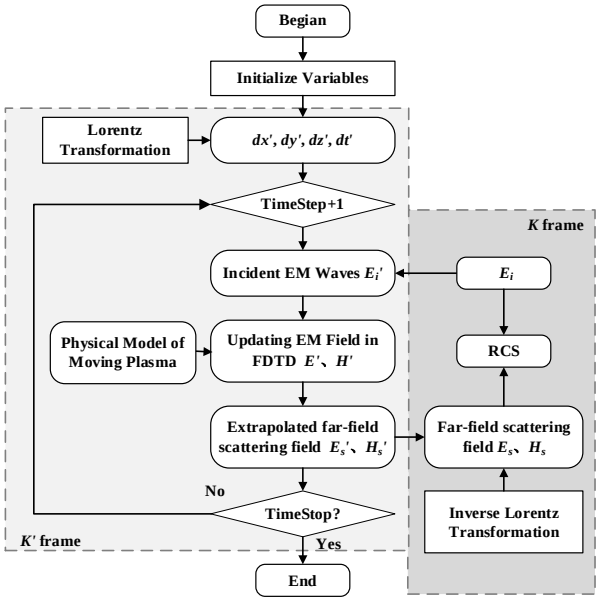

Fig. 2. Flowchart of Lorentz-FDTD algorithm for the calculation of motion dispersion media.

the EM wave frequency ω' after the Doppler shift can be calculated as [16]

$$\omega' = \gamma\omega(1-\beta\cos\theta), \tag{1}$$

where $\gamma = 1/\sqrt{1-\beta^2}, \beta = v/c$. c is the velocity of light in free space.

The dielectric coefficient ε_r of a magnetized cold plasma is generally described using Appleton's formula.

$$\varepsilon_r(\omega) = 1 - \frac{\omega_p^2}{\omega^2+\omega_c^2} - j\frac{\omega_c}{\omega}\frac{\omega_p^2}{\omega^2+\omega_c^2}, \tag{2}$$

where ω_p is the plasma cut-off frequency and ω_c is the plasma collision frequency. ω is the operating frequency of EM waves.

The EM wave frequency ω' in the K' frame will be red-shifted when the object moves away from the detection radar radiation. Conversely, the ω' will be blue-shifted when the object is moves toward the direction of

EM wave propagation. Therefore, the dielectric coefficient ε_r of plasma in the K' frame can be further written as

$$\varepsilon_r'(\omega') = 1 - \frac{\omega_p^2}{\omega'^2 + \omega_c^2} - j\frac{\omega_c}{\omega'}\frac{\omega_p^2}{\omega'^2 + \omega_c^2}. \quad (3)$$

The EM field update equation for a moving plasma based on the shift-operator (SO-FDTD) method [20–22] is derived as follows. First, as the dielectric coefficient of the plasma will change with the EM wave frequency, the electric field frequency domain intrinsic relationship of the moving plasma can be expressed as

$$\boldsymbol{D}'(\omega') = \varepsilon_0 \varepsilon_r'(\omega')\boldsymbol{E}'(\omega'), \quad (4)$$

where the rational fraction of ε_r in the SO-FDTD method is expressed in the form

$$\varepsilon_r'(\omega') = \frac{\sum_{n=0}^{N} p_n (j\omega')^n}{\sum_{m=0}^{M} q_m (j\omega')^m}, \quad (5)$$

where p_n and q_n denote the numerator and denominator coefficients of the relative permittivity, respectively.

To simplify the equation, we define the velocity factor $C=\gamma(1-\beta\cos\theta)$, then establish the equation $j\omega'=C\,j\omega$. The time domain forms of the electric field and relative dielectric coefficients of plasma can be transitioned by the conversion operator $j\omega = \partial/\partial t$ between the time and frequency domains. Therefore, the time-domain form of (5) can be deduced further as

$$\varepsilon_r'\left(\frac{\partial}{\partial t'}\right) = \frac{\sum_{n=0}^{N} p_n C^n (\frac{\partial}{\partial t})^n}{\sum_{m=0}^{M} q_m C^m (\frac{\partial}{\partial t})^m}. \quad (6)$$

The time-domain intrinsic form of the electric field can be acquired by bringing (6) into the electric field intrinsic structure relation (4).

$$\left[\sum_{m=0}^{M} q_m C^m \left(\frac{\partial}{\partial t}\right)^m\right]\boldsymbol{D}'(t') = \varepsilon_0\left[\sum_{n=0}^{N} p_n C^n \left(\frac{\partial}{\partial t}\right)^n\right]\boldsymbol{E}'(t'). \quad (7)$$

By discretizing the time derivative in (7) with the central difference $\left(\frac{\partial}{\partial t}\right)^l \to \left(\frac{2}{\Delta t}\cdot\frac{z_t-1}{z_t+1}\right)^l$, where z_t denotes the discrete time-domain shift operator and l represents the order of time derivative [21]. The electric field update equation in the SO-FDTD method is given by

$$\begin{aligned}&\left\{\left[q_0' + q_1'\frac{2}{\Delta t} + q_2'\left(\frac{2}{\Delta t}\right)^2\right]z_t^2 + \left[2q_0' - 2q_2'\left(\frac{2}{\Delta t}\right)^2\right]z_t + \right.\\ &\left.\left[q_0' - q_1'\frac{2}{\Delta t} + q_2'\cdot\left(\frac{2}{\Delta t}\right)^2\right]\right\}\boldsymbol{D}_x'^n =\\ &\left\{\left[p_0' + p_1'\frac{2}{\Delta t} + p_2'\left(\frac{2}{\Delta t}\right)^2\right]z_t^2 + \left[2p_0' - 2p_2'\left(\frac{2}{\Delta t}\right)^2\right]z_t + \right.\\ &\left.\left[p_0' - p_1'\frac{2}{\Delta t} + p_2'\left(\frac{2}{\Delta t}\right)^2\right]\right\}\varepsilon_0\boldsymbol{E}_x'^n. \end{aligned} \quad (8)$$

The differential form of the electric field update equation for a moving dispersive medium is as follows:

$$\begin{aligned}\boldsymbol{E}'^{n+1} = \frac{1}{b_0}\left\{\frac{1}{\varepsilon_0}\left(a_0\boldsymbol{D}'^{n+1} + a_1\boldsymbol{D}'^{n} + a_2\boldsymbol{D}'^{n-1}\right)\right.\\ \left. - b_1E'^n - b_2E'^{n-1}\right\},\end{aligned} \quad (9)$$

where the coefficients $a_0, a_1, a_2, b_0, b_1, b_2$ are as follows:

$$\begin{cases} a_0 = q_0' + q_1'\left(\frac{2}{\Delta t}\right) + q_2'\left(\frac{2}{\Delta t}\right)^2, & b_0 = p_0' + p_1'\left(\frac{2}{\Delta t}\right) + p_2'\left(\frac{2}{\Delta t}\right)^2 \\ a_1 = 2q_0' - 2q_2'\left(\frac{2}{\Delta t}\right)^2, & b_1 = 2p_0' - 2p_2'\left(\frac{2}{\Delta t}\right)^2 \\ a_2 = q_0' - q_1'\left(\frac{2}{\Delta t}\right) + q_2'\left(\frac{2}{\Delta t}\right)^2, & b_2 = p_0' - p_1'\left(\frac{2}{\Delta t}\right) + p_2'\left(\frac{2}{\Delta t}\right)^2 \end{cases}, \quad (10)$$

where $q_n' = C^n q_n$, $p_n' = C^n p_n$ $(n = 0,1,2)$, and the coefficients q_n and p_n are determined by the EM parameters of plasma.

B. Lorentz transformation of space-time increments

When the Lorentz transformation is introduced into the FDTD method according to the principle of special relativity, the relationship between the space-time increments of two inertial systems satisfy the Lorentz transformation equation. Suppose that the K' frame is moving with constant velocity $\vec{v}$ relative to the K frame, and the origin of the two frames coincide at the instantaneous moment $t = t' = 0$. The space-time increment between the two inertial frames is given by (11).

$$\begin{pmatrix}\Delta x\\ \Delta y\\ \Delta z\end{pmatrix} = \begin{pmatrix} 1+(\gamma-1)\frac{v_x^2}{v^2} & (\gamma-1)\frac{v_xv_y}{v^2} & (\gamma-1)\frac{v_xv_z}{v^2} \\ (\gamma-1)\frac{v_xv_y}{v^2} & 1+(\gamma-1)\frac{v_y^2}{v^2} & (\gamma-1)\frac{v_yv_z}{v^2} \\ (\gamma-1)\frac{v_xv_z}{v^2} & (\gamma-1)\frac{v_yv_z}{v^2} & 1+(\gamma-1)\frac{v_z^2}{v^2} \end{pmatrix} \cdot \begin{pmatrix}\Delta x'\\ \Delta y'\\ \Delta z'\end{pmatrix}, \quad (11\text{-a})$$

$$\Delta t = \frac{1}{\sqrt{1-\beta^2}}(1 - \beta\hat{a}_s\cdot\hat{a}_v)\Delta t', \quad (11\text{-b})$$

where $v_x = |\vec{v}|\sin\theta_v\cos\varphi_v, v_y = |\vec{v}|\sin\theta_v\sin\varphi_v$, $v_z = |\vec{v}|\cos\theta_v$. θ_v is the elevation angle of $\vec{v}$ with $+z$ axis, φ_v is the angle between the projection of $\vec{v}$ on xOy and $+x$ axis. The symbol $\hat{a}_s$ and $\hat{a}_v$ denotes the unit vectors of the scattered field and velocity, respectively.

C. Incident EM field transformation

In order to solve the dynamic EM problem for high-speed targets by the FDTD method, the incident plane EM wave in the K frame need to be converted to the K' frame. Assume that the unit vector of incident EM wave propagating along arbitrary direction in the K frame is defined as $\overrightarrow{k}_i$. According to the phase-invariant principle of EM waves [23], the wave vector $\overrightarrow{k}_i'$, angular frequency ω_i' and amplitude $\overrightarrow{E}_i'$transformation equations of

the incident plane EM wave in the K' frame are given by (12)-(14).

$$\vec{\mathrm{k}}_i^{'} = \gamma\vec{\mathrm{k}}_i\left(1-\beta\frac{\vec{\mathrm{k}}_i\cdot\vec{\mathrm{v}}}{|\vec{\mathrm{v}}|}\right), \tag{12}$$

$$\omega_i^{'} = \gamma\omega_i\left(1-\beta\frac{\vec{\mathrm{k}}_i\cdot\vec{\mathrm{v}}}{|\vec{\mathrm{v}}|}\right), \tag{13}$$

$$|\vec{E}_i^{'}| = \sqrt{(\vec{E}_0\cos\theta)^2+\gamma^2(\vec{E}_0\sin\theta+|\vec{v}\times\vec{B}|)^2}, \tag{14}$$

where the ω_i, $\vec{E}_0$are the angle frequency and amplitude of the incident EM waves in the K frame.

D. Near- to far-field extrapolation

In the frame K', the near-field scattered field of the moving target can be obtained by using the time domain EM field iteration of conventional FDTD. The far-field scattered EM field can be obtained by extrapolation from the near-field data. First, a closed virtual boundary is set as the extrapolation boundary in the FDTD scattering field region according to the equivalence principle. Second, the tangential current and tangential magnetic current on the virtual boundary are calculated, and the equivalent EM current on this surface is extrapolated according to the Huygens's principle. In addition, the 10-level uniaxial anisotropy perfectly matched (UPML) layer as absorbing boundary is used to terminate the outward propagating EM field in space. The 3D far-field equation in the frame K' can be expressed as

$$\begin{aligned} e_\theta^{s'}(t') = {} & u_x'\sin\varphi_s' - u_y'\cos\varphi_s' - \eta\left(w_x'\cos\theta_s'\cos\varphi_s'\right. \\ & \left. + w_y'\cos\theta_s'\sin\varphi_s' - w_z'\sin\theta_s'\right) \end{aligned}, \tag{15-a}$$

$$\begin{aligned} e_\varphi^{s'}(t') = {} & u_x'\cos\theta_s'\cos\varphi_s' + u_y'\cos\theta_s'\cos\varphi_s' - u_z'\sin\theta_s' \\ & + \eta\left(w_x'\sin\varphi_s' - w_y'\cos\varphi_s'\right) \end{aligned}, \tag{15-b}$$

where η is the wave impedance in free space. $\boldsymbol{w}'(t)$ and $\boldsymbol{u}'(t)$ can be obtained by performing the inverse Fourier transform on (16).

$$\begin{aligned} \overrightarrow{\boldsymbol{W}}' &= jk\rightarrow\mathbf{A}' \\ &= jk\frac{\exp(-jk'r')}{4\pi r'}\int_A\left(\hat{n}\times\rightarrow\mathbf{H}_s'\right)\exp\left(jk'\boldsymbol{r}'\cdot\hat{\boldsymbol{e}}_{r'}'\right)ds' \end{aligned}, \tag{16-a}$$

$$\begin{aligned} \overrightarrow{\boldsymbol{U}}' &= jk\overrightarrow{\boldsymbol{F}}' \\ &= jk\frac{\exp(-jk'r')}{4\pi r'}\int_A-\left(\hat{n}\times\overrightarrow{\boldsymbol{E}}_s'\right)\exp\left(jk'\boldsymbol{r}'\cdot\hat{\boldsymbol{e}}_{r'}'\right)ds' \end{aligned}, \tag{16-b}$$

E. Inverse Lorentz transformation of EM field

As the Maxwell system of equations satisfies the covariance principle, its rotational equations remain in the same form in all inertial systems. Therefore, Maxwell's rotational equations in K' can be expressed as

$$\frac{\partial\vec{\boldsymbol{D}}^{'}}{\partial t'} = \nabla\times\vec{\boldsymbol{H}}^{'}, \tag{17}$$

$$\frac{\partial\vec{\boldsymbol{H}}^{'}}{\partial t'} = -\frac{1}{\mu_0}\nabla\times\vec{\boldsymbol{E}}^{'}. \tag{18}$$

In the previous section, the far-field scattered fields $\overrightarrow{\boldsymbol{E}}_{s\theta}'$ and $\overrightarrow{\boldsymbol{E}}_{s\varphi}'$ of the high-speed target were obtained by near to far-field extrapolation. The electric and magnetic field components will change in the two inertial systems due to the relative motion between the K frame and the K' frame. The relationship between the EM fields in the two frames follows the Lorentz transformation equation. The inverse Lorentz transformation equation for the far-field scattered EM field between two frames is given by (20)-(21).

$$\vec{\boldsymbol{E}} = \gamma(\vec{\boldsymbol{E}}^{'}-\vec{v}\times\vec{\boldsymbol{B}}^{'})+(1-\gamma)\frac{\vec{\boldsymbol{E}}^{'}\cdot\vec{v}}{v^2}\vec{v}, \tag{19}$$

$$\vec{\boldsymbol{B}} = \gamma(\vec{\boldsymbol{B}}^{'}-\frac{1}{c^2}\vec{v}\times\vec{\boldsymbol{E}}^{'})+(1-\gamma)\frac{\vec{\boldsymbol{B}}^{'}\cdot\vec{v}}{v^2}\vec{v}, \tag{20}$$

where spatial electric field $\overrightarrow{\boldsymbol{E}}'$ and magnetic field $\overrightarrow{\boldsymbol{B}}'$ are represented in FDTD with Cartesian coordinates. Therefore, the far-field $\overrightarrow{\boldsymbol{E}}_{sx}'$, $\overrightarrow{\boldsymbol{E}}_{sy}'$, $\overrightarrow{\boldsymbol{E}}_{sz}'$ can be obtained by performing a coordinate transformation on $\overrightarrow{\boldsymbol{E}}_{s\theta}'$ and $\overrightarrow{\boldsymbol{E}}_{s\varphi}'$. In the SO-FDTD method, the far-field scattered field in the K frame is derived as follows. The Lorentz transformation equation of the spatial electric field in FDTD is given below.

$$\begin{aligned} \begin{pmatrix}\overrightarrow{\boldsymbol{E}}_x\\ \overrightarrow{\boldsymbol{E}}_y\\ \overrightarrow{\boldsymbol{E}}_z\end{pmatrix} &= \gamma\begin{pmatrix}\overrightarrow{\boldsymbol{E}}_x'\\ \overrightarrow{\boldsymbol{E}}_y'\\ \overrightarrow{\boldsymbol{E}}_z'\end{pmatrix}-\gamma\begin{pmatrix}\hat{x} & \hat{y} & \hat{z}\\ v_x & v_y & v_z\\ \overrightarrow{\boldsymbol{B}}_x' & \overrightarrow{\boldsymbol{B}}_y' & \overrightarrow{\boldsymbol{B}}_z'\end{pmatrix} \\ &\quad+(1-\gamma)\frac{\overrightarrow{\boldsymbol{E}}_x'v_x+\overrightarrow{\boldsymbol{E}}_y'v_y+\overrightarrow{\boldsymbol{E}}_z'v_z}{v^2}\overrightarrow{\boldsymbol{v}}. \end{aligned} \tag{21}$$

The frequency domain field value $\overrightarrow{E}_i(f)$ of the incident EM wave can be obtained by Fourier transforming the time domain incident field $\overrightarrow{E}_i(t)$. The 3D radar scattering cross section (RCS) can be calculated by (25).

$$\mathrm{RCS}(f) = \lim_{r\to\infty}\left\{10\log\left(4\pi r^2\left|\frac{\vec{E}_s(f)}{\vec{E}_i(f)}\right|^2\right)\right\}. \tag{22}$$

F. Stability and dispersion

It is necessary to ensure the stability and dispersion stability of Lorentz–FDTD method in the analysis the moving target coated with plasma sheath. Assume the time and space grids of the Lorentz–FDTD in the frame K' are set to $dx' = dy' = dz' = \delta$ and $dt' = \delta/2c$. The Courant stability criterion for the FDTD in the K' frame

is given by equation (23), according to the principle of invariance of the speed of light [22]:

$$\Delta t' \le \frac{\delta}{\sqrt{3}c}. \tag{23}$$

Given that the EM wave will be modulated by the velocity of the target and the effect of strong dispersion of the plasma, to guarantee the dispersion stability of the FDTD is necessary, and it can be achieved by selecting a suitable spatial increment δ. The spatial grid parameters to satisfy the FDTD dispersion stability in the frame K' are given in (24) [23]:

$$\delta \le \frac{\lambda'}{12}, \tag{24}$$

where λ' is the minimum wavelength in plasma sheath corresponding to the maximum frequency after the blue-shift of the EM wave, which can be calculated according to the frequency-resolved formula for the scattered field of a moving target [16]. Equation (24) reveals that the velocity of the object affects the EM wave frequency and thus imposes certain restrictions on the spatial grid of the FDTD. In turn, the maximum frequency f_{max} that can be calculated with the FDTD is determined once the space-time increments are set. Therefore, the dispersion stability of the FDTD can be guaranteed when the velocity is less than the critical velocity (herein, the critical velocity is defined as the maximum frequency equal to the f_{max} after the blue-shift of the EM wave frequency caused by the target moving at that velocity). Simulating higher velocities of the moving object can be achieved by reasonably reducing the space-time increments of the FDTD.

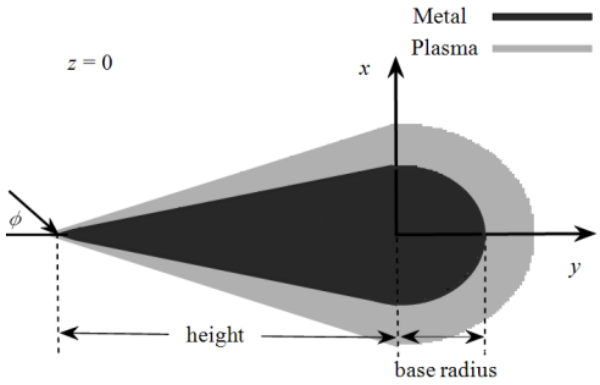

Fig. 3. Shape of cone-sphere target is in the xOy plane.

III. VALIDITY AND ACCURACY

A. Validation of Lorentz-FDTD method

As a validation example, the monostatic RCS of a high-speed moving metal sphere with radius of 1 m is calculated using the proposed algorithm. The space-time increment of Lorentz-FDTD is set to $dx'= dy'= dz'=$ 0.05 m and $dt'= dx'/ 2c$. In frame K', the incident plane EM wave is a Gaussian pulse source is defined with the parameters of $\tau = 40dt'$ and $t_0 = \tau$. The EM propagation angles are set to $\theta_i = 90^\circ$ and $\varphi_i = 90^\circ$, and the incident electric field is polarization along the $+z$-direction. This target is moving with the velocity v of $0.1c$ along the direction of θ_v=90° and φ_v=90°.

Figure 4 presents the comparison of the RCS results calculated in this article with the RCS results in [23]. It can be seen in Fig. 4 that the RCS of the moving metal sphere complies perfectly with the results in [23] in terms of the variation pattern with the EM wave frequency when the target moves at velocity v of 0 and $0.1c$. The maximum error between the two results of RCS is less than 2.0 dB, which can be a good verification of the proposed algorithm in the analysis scattered fields from moving targets.

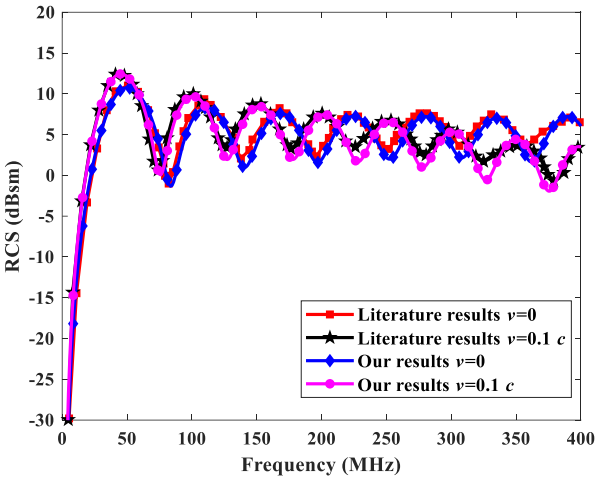

Fig. 4. The monostatic RCS from moving metal sphere target compared with the RCS results in literature.

B. Accuracy in analysis of moving dispersive medium

Here, we adopt a plasma sphere with a diameter of 7.5 mm as a validation example for dispersive media, where the plasma frequency ω_p is 1.8×10^{11} rad/s and the collision frequency ω_c is 20 GHz. The Lorentz–FDTD method is used to calculate the monostatic RCS of the plasma sphere, and the results would be compared with that calculated with Mie theory to verify the validity and accuracy of the proposed algorithm in analyzing EM scattering from dispersive-medium objects. The spatial and time increments of the Lorentz–FDTD are set as $dx'= dy'= dz'=$ 0.05 mm and $dt'= dx'/ 2c$. A Gaussian pulsed plane wave with a pulse width τ of $60dt'$ is incident along the directions $\theta_i = \pi / 2$ and $\varphi_i = \pi / 2$.

Figure 5 presents the results of monostatic RCS calculated with the Lorentz–FDTD and Mie theory

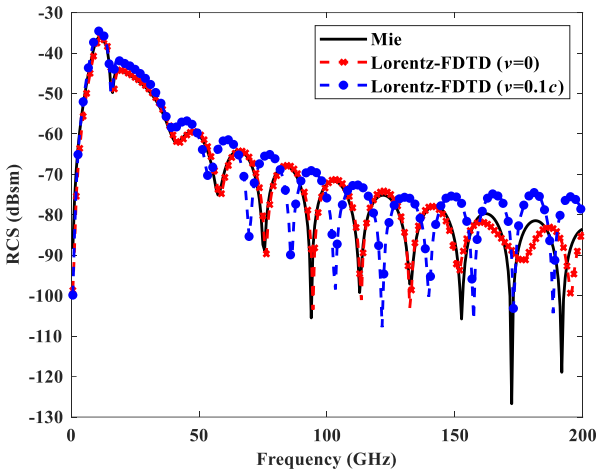

Fig. 5. The monostatic RCS from moving plasma sphere target compared with the Mie's resolution.

respectively for the plasma sphere. From Fig. 5, we can see that when the plasma target is stationary, the RCS results calculated with two methods are nearly consistent. When the plasma target moves away from the incident EM wave source with a velocity of $0.1c$, the monostatic RCS is significantly modulated toward lower frequencies by the motion property of the plasma target, which can be conformed to the expected Doppler effect.

IV. NUMERICAL RESULTS

A. High-speed moving metal cone-sphere target

In this section, the EM scattered properties of a 3D metal cone-sphere target without plasma sheath coating are investigated. The cone-sphere target has a height of 15 cm and base radius of 5 cm. The model of this target in the xOy plane is shown in Fig. 3. The time and space increment of Lorentz–FDTD are set to $dx' = dy' = dz' = \lambda/20$ and $dt' = dx'/2c$, where $\lambda = c/f_0$ is the wavelength of the EM wave at the modulation frequency. The simulation space is defined as $T_x \times T_y \times T_z = (180 \times 180 \times 180)\delta$. The incident plane wave source is a modulated Gaussian pulse with the parameters of center frequency of $f_0 = 4$ GHz, bandwidth of $B = 4$ GHz, pulse width of $\tau = 1.7/B$, and time delay of $t_0 = 0.8\tau$. The plane EM wave was introduced in the SO-FDTD method by using the 3D TF-SF boundary based on the equivalence principle. The mathematical expression of the incident signal is given in

$$E_i'(t') = E_0' \cos\left(2\pi f_0' t'\right) \exp\left(-\frac{4\pi\gamma_t^2 (t'-t_0)^2}{\tau^2}\right), \quad (25)$$

where the E_0' is the amplitude of incident wave in the K'frame, and $\gamma_t = \gamma(1 - \beta\cos\theta)$. The direction of incidence is $\theta_i = 90^\circ$ and $\varphi_i = 90^\circ$, the polarization angle α is set to 90°, the receiving angle $\theta_s = 90^\circ$ and $\varphi_s = 270^\circ$. The corresponding calculation time to update EM field components 3×10^3 times is 0.5 h by using a microcomputer.

Figure 6 shows the backscattering properties of the target with different velocities. The results in Fig. 6 (a) illustrate that when the target moves along the incident direction, the scattered waves in the time domain are delayed and the amplitude decreases slightly, whereas the opposite phenomenon is observed when moving close to the incident wave. In Fig. 6 (a), as the target moves away from the incident wave at $v = 0.02c$, the scattered waveform received in the time domain delays about 0.075 ns compared with that received when the target is stationary. And the time delay will be 0.15 ns for the receding velocity v of $0.04c$. Conversely, the

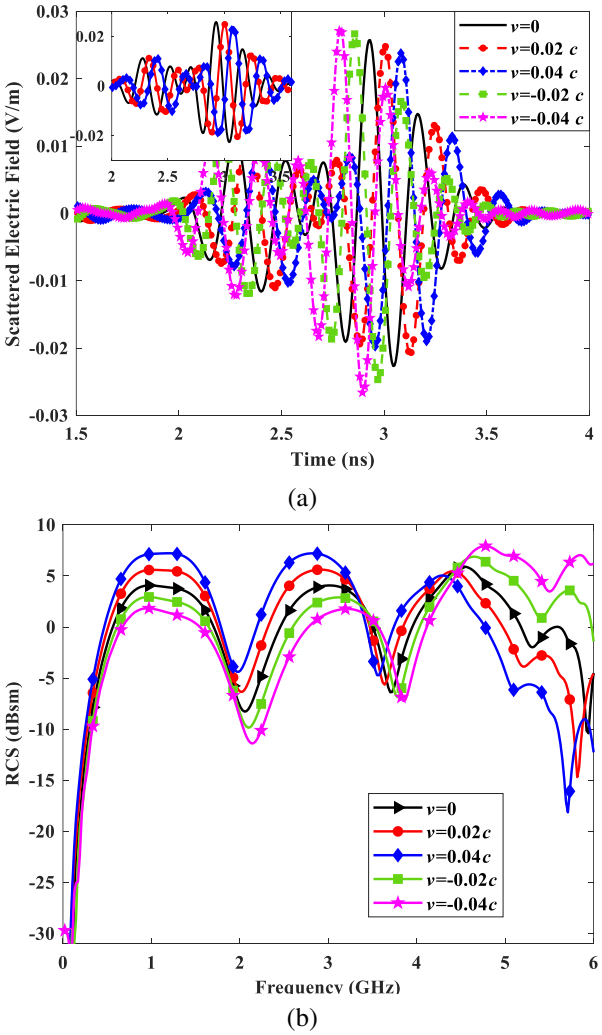

Fig. 6. Scattering fields radiated from a metallic cone-sphere target with motion direction as $\theta_v = 90^\circ$ and $\varphi_v = 90^\circ$: (a) Scattering field in the time domain and (b) monostatic RCS.

scattered waveform in the time domain will advance by about 0.075 ns for v of $0.02c$ when the target is moving close to the incident source. Further simulations reveal that the time delay of the scattered waveform caused by the motion will differ if the shape of the target is changed. As shown in Fig. 6 (b), the monostatic RCS has a frequency shift toward the low-frequency band if the object moves along the incident direction ($v > 0$). Conversely, RCS has a frequency shift to the high-frequency band while the target moves toward the incident waves ($v < 0$).

For a high-speed moving rotating target, the EM scattering strongly depends on its state of motion, orientation, and shape [14]. To further investigate the relationship between the backward echo characteristics and the velocity of a moving target, the EM echoes of a high-speed moving-cone-sphere target are simulated for different ratios, where the ratio is defined as *ratio = height / base radius*. The details of the target dimensions at different ratios are given in Table 1. The incident wave is incident along the tip of the moving target, and the distance of the plane wave to each cone tip is ensured to be constant.

Table 1: Dimension parameters of cone-sphere target

Ratios	Height (cm)	Base Radius (cm)
0.1	1.5	15
0.5	5.5	11
1.0	17	17
5.0	25	5
10	34	3.4

Figure 7 (a) shows the time-domain waveform of the incident signal. Figures 7 (b)-(f) present the time tracks of backscattered pulse fields of the cone-sphere targets with different ratios and at different velocities. The result in Fig. 7 shows that the backscattered waveform from the target contains abundant information about the target. First, the variation of the scattered wave in terms of delay and amplitude reflects the motion velocity of the object. Second, the waveform variation of the scattered field in the time domain is strongly correlated with the ratio of the target. The maximum amplitude of the scattered field decreases with the target ratio raising, and the scattered field lags significantly in the time domain. For the different ratios and same motion velocity of target, the time delay of the scattered field from the targets has a big difference, and the degree of time delay slightly increases with ratio enlarging. However, as the velocity is $0.04c$, the time delay (compared with the stationary target) is twice as long as that when the velocity is $0.02c$ for all cone ratios.

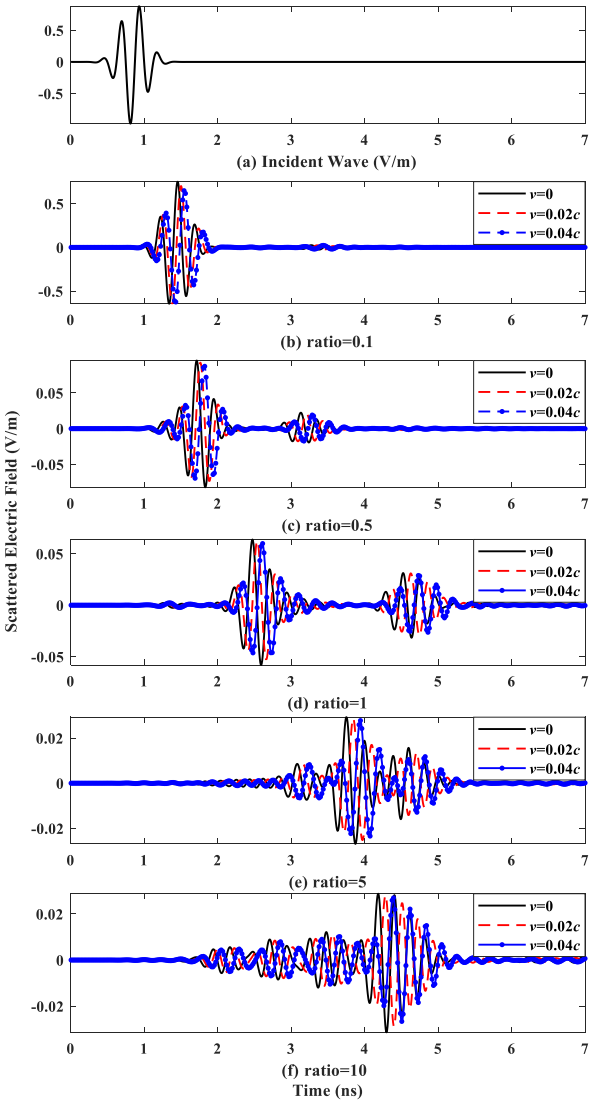

Fig. 7. The incident signal and backscattered waveform of moving cone-sphere targets with different ratios.

B. Moving cone-sphere target coated with plasma sheath

In this section, the influence of the typical EM characteristic parameters of the plasma sheath on the scattered field of the moving cone-sphere target is studied by referring to the measured data of the flow field around a high-speed vehicle [26–27]. A modulated Gaussian pulse source with parameters of f_0 = 4 GHz, B = 4 GHz, τ = 1.7 / B, and $t_0 = 0.8\tau$ is applied to irradiate the moving target. The space-time increment of Lorentz–FDTD are set to $dx' = dy' = dz' = \lambda$ / 54 and $dt' = dx'/2c$. The cone-sphere target with a height of 0.045 m and a base radius of 0.015 m moves at $0.01c$ along the $+y$ axis. The direction of incident wave is $\theta_i = 90^\circ$ and $\varphi_i = 90^\circ$ in

Table 2: EM parameters of the plasma sheath

Case	Electron Density n_e ($\times$ 1016 m^{-3})	Collision Frequency ω_c (GHz)	Incident Angle ϕ_i (°)
a	1, 5, 10, 20, 100	20	0
b	10	1,5, 10, 20	0
c	20	5	0, 30, 45, 60

simulations of case (a) and (b). In simulation of case (c), the angle of incidence $\theta_i = 90°$, and φ_i is given in Table 2. The EM parameters of the plasma sheath and incident angle are given in Table 2. In additional, the calculation time for the computer to update EM field 4.2×10^3 times is 0.8 h.

Figure 8 displays the variation in monostatic RCS under different plasma electron densities when the target moves at $0.01c$ along the $+y$ axis. It can be seen that the monostatic RCS varies substantially at different electron densities because the cut-off frequency of plasma increases as electron density increases. When the operating frequency of the EM wave is less than the cut-off frequency of plasma ($f < 2$ GHz), the backscattering ability of the plasma sheath for EM waves increases with increased electron density. Therefore, monostatic RCS increases with increased electron density in the low-frequency band. However, when the operation frequency is greater than the cutoff frequency of plasma (f belongs to 2-12 GHz), the reflection caused by plasma decreases, and the absorption of EM waves increases. Eventually, RCS decreases rapidly as electron density increases. Moreover, the maximum absorption position of the RCS for EM waves gradually shifts toward high frequencies with the increase in electron density. When the electron density of plasma is set to 1×10^{18} m^{-3}, the cut-off frequency of plasma is greater than other values, but monostatic RCS decreases very rapidly. This finding is due to most of the EM waves being scattered in the forward-scattering direction, thereby causing a rapid decrease in backscattering direction.

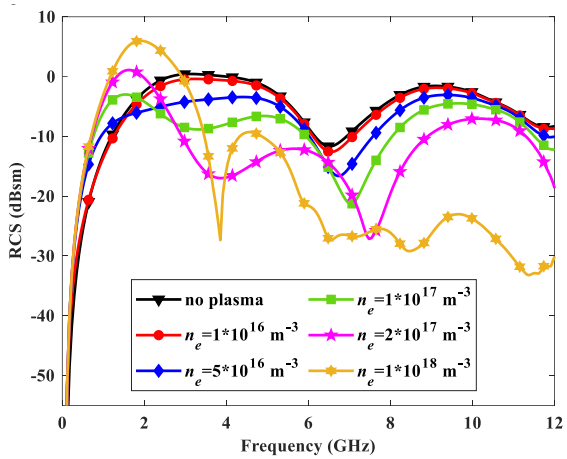

Fig. 8. Monostatic RCS of cone-sphere target coated by plasma sheath with different electron densities n_e.

Figure 9 shows the change in monostatic RCS under different plasma collision frequencies ω_c. When the EM wave operating frequency f ranges within 0-2 GHz, monostatic RCS increases with decreased collision frequency. RCS has a more dramatic change with collision frequency when the plasma frequency is close to the cut-off frequency of EM waves. When the operating frequency f is 2-4 GHz, monostatic RCS decreases first and then increases with increased collision frequency, and decay is maximum at collision frequency $\omega_c = 5$ GHz. This finding is due to that the absorption of EM waves is more remarkable by the plasma sheath when collision frequency wave is close to the cut-off frequency. The monostatic RCS decreases rapidly with increased collision frequency when the operating frequency is greater than the cut-off frequency.

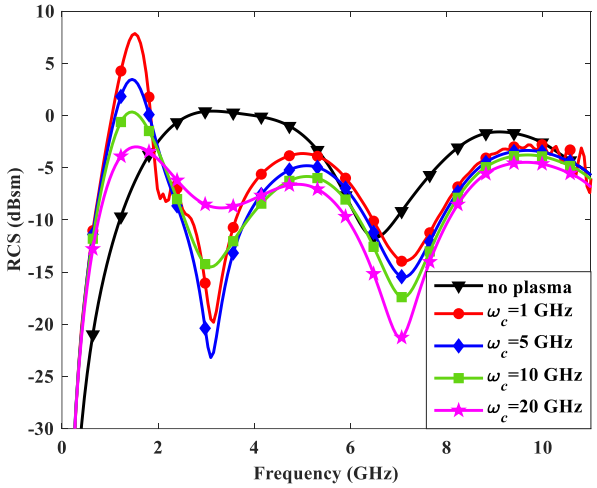

Fig. 9. Monostatic RCS of cone-sphere target coated by plasma sheath with different collision frequencies ω_c.

Figure 10 shows monostatic RCS variation with the angle of the incident wave. The angle of the incidence plane wave has a remarkable effect on monostatic RCS when the operating frequency f ranges within 2-5 GHz. In this frequency range, RCS increases significantly as the incident angle increases. This is mainly because the frequency of EM waves is close to the cut-off frequency, and in this condition the direction of incidence of EM waves has a greater influence on the monostatic RCS. However, the monostatic RCS does not increase with the increase of the incident angle when the operating frequency of EM waves is higher than the cut-off frequency ($f > 6$ GHz).

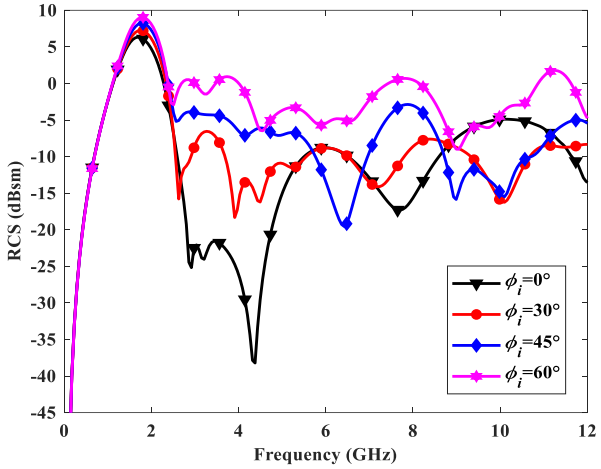

Fig. 10. Monostatic RCS of cone-sphere target coated by plasma sheath with different angles ϕ_i of incident wave.

To illustrate the effect of the electron density of a plasma sheath at different operating frequencies on the EM-scattering ability of the moving cone-sphere target, the bistatic RCS of the cone-sphere target varies with different electrons at different operating frequencies f of 1, 4, and 9 GHz. The operating frequency f = 1 GHz is less than the plasma frequency, f = 4 GHz is within the range of plasma frequency, and f = 9 GHz is greater than the plasma frequency. The collision frequency ω_c of the plasma sheath is 20 GHz, and the thickness of the plasma sheath is 1 cm. The target moves along the $+y$ axis with velocity $0.01c$. The plane wave is incident in the direction of $\theta_i = 90°$ and $\varphi_i = 90°$, and the electric field is polarized along the $+z$ direction. When the scattering angle $\theta_s = 90°$, the bistatic RCS in the xOy scattering plane is observed. The bistatic RCS of moving the cone-sphere target at different operation frequencies of EM waves is shown in Fig. 9.

Figure 11 (a) shows that bistatic RCS increases with the increase electron densities of plasma sheath in both the forward-scattering direction $\varphi_s = 90°$ and the backscattering direction $\varphi_s = 270°$. The increased reflection of the EM wave is caused by the increased electron densities of the plasma sheath when the operating frequency f is less than the plasma cutoff frequency. In Fig. 11 (b), the bistatic RCS increases as the electron densities increases in the forward-scattering direction at $\varphi_s = 90°$. In the backscattering direction at φ_s =270°, the RCS reaches its minimum when the electron densities $n_e = 2\times10^{17}$ m^{-3}. This occurs because the cutoff frequency of plasma at electron densities $n_e = 2 \times 10^{17}$ m^{-3} matches the operating frequency of EM waves, leading to the most pronounced absorption of EM waves by the plasma. Figure 11 (c) shows that the bistatic RCS in the forward-scattering direction $\varphi_s = 90°$

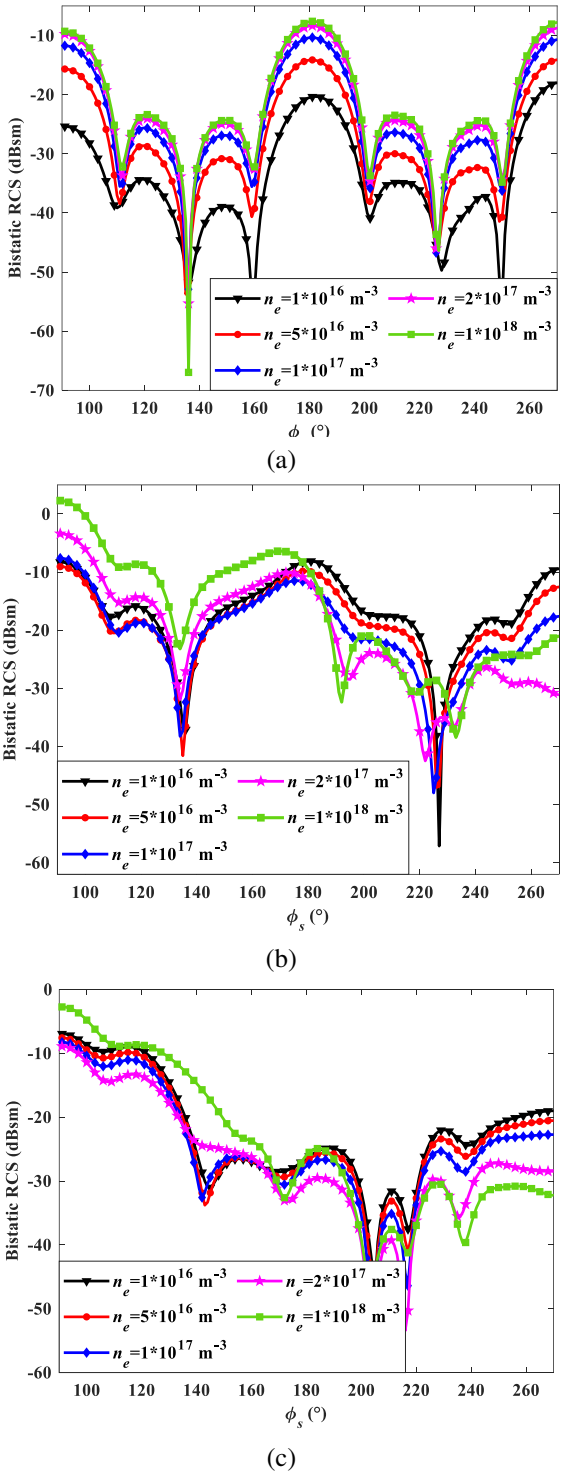

Fig. 11. (a) HIS structure and (b) Equivalent circuit.

decreases with increased electron densities when $n_e \leq 2 \times 10^{17}$ m^{-3}, but increases at $n_e = 1 \times 10^{18}$ m^{-3} and decreases rapidly with increasing electron density in the backscattering direction $\varphi_s = 270°$. The RCS changes

more considerably in the backscattering direction than in the forward-scattering one. Figure 8 (a) can be verified again. When the electron density $n_e = 1 \times 10^{18}$ m^{-3}, the reason for the rapid decreases of monostatic RCS at high frequencies is that the EM wave is scattered to the forward-scattering direction.

C. Doppler effect on scattered field

In this section, we examine the impact of the velocity on the Doppler effect of the scattered field of a high-speed target. The parameters of the FDTD grid and the dimensions of the target are the same as in Section B. The EM parameters of the plasma sheath are set as the electron density n_e of 3×10^{16} m^{-3} and 3×10^{17} m^{-3}, ω_c of 10 GHz, and a plasma thickness of 1 cm. The incident direction is set to $\theta_i = \pi/2$ and $\varphi_i = \pi/2$. This object is moving at velocities v of 0.02c, 0.04 c, -0.02c, and -0.04c along the incident direction.

It is evident from Fig. 12 that the RCS experiences a red-shift when the target moves away the incident wave ($v > 0$) and a blue-shift when the target moves toward the source. This phenomenon bears resemblance to the frequency modulation law observed in moving metal targets. However, the complexity of the amplitude modulation law increases. Due to the variation in electron density, the RCS exhibits different levels of reduction across various frequency bands of EM waves. As depicted in Fig. 12 (a), when the electron density $n_e = 3 \times 10^{16}$ m^{-3}, the operation frequency f of EM waves significantly exceeds the cut-off frequency of the plasma. Therefore, there is a lower absorbing and higher scattering of plasma on the EM waves. Figure 12 (b) presents the variation of RCS with velocity when the electron density $n_e = 3 \times 10^{17}$ m^{-3}. It can be seen that when the operation frequency f is in the range of 3.5-5.0 GHz, the RCS when the velocity v of 0.04 c is significantly stronger than at the velocity v of -0.04 c. This finding is due to the variations of the target velocity changes the relative dielectric coefficient of plasma, which in turn influences the absorbing and scattering of plasma on EM waves. With the target moving away from the source, the red-shift will decrease the frequency of EM waves, which increases the scatter of plasma on EM waves. By contrast, the blue-shift due to the target moving toward the source will increase the EM wave frequency, which increases the absorbing of plasma on EM waves. The scattering EM echo from this plasma coated target at different velocities is presented in Fig. 13.

Finally, to investigate the impact of velocity on the Doppler shift of the scattered field from the target, a time-harmonic signal with a carrier frequency of 4 GHz was used to irradiate the target. The backscattered field in the time domain was then recorded. Further, the analysis of the variation of Doppler shift with object velocity

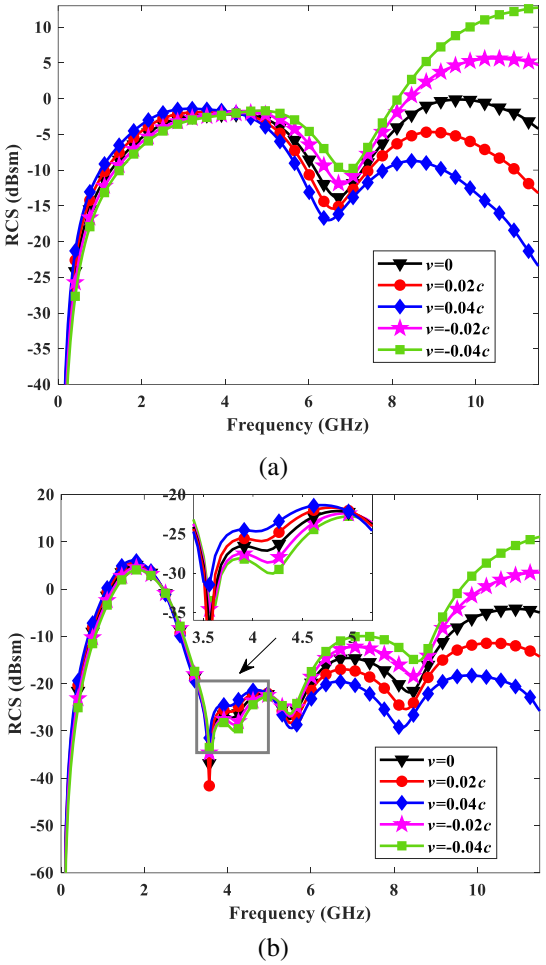

Fig. 12. Monostatic RCS in different velocities when the target coated with a plasma sheath with electron densities (a) n_e=3×10^{16} m^{-3} and (b) n_e=3×10^{17} m^{-3}.

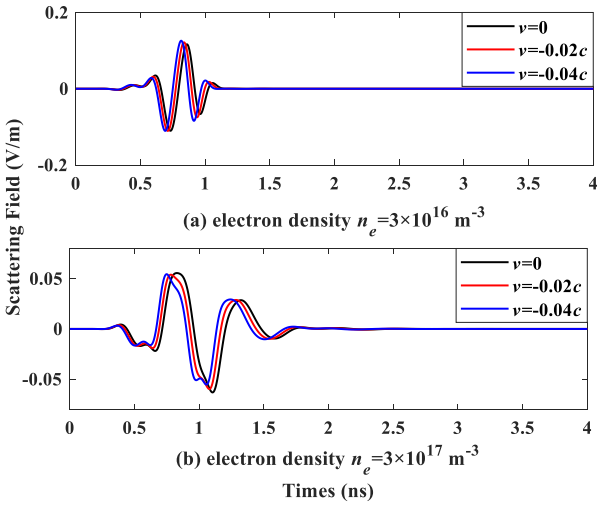

Fig. 13. EM echo in different velocities when the plasma coated target with electron densities n_e of 3×10^{16} and 3×10^{17} m^{-3}.

Table 3: Doppler shift and relative error of scattered field in different velocities

Velocity	Numerical Results (GHz)	Theoretical Results (GHz)	Error
0.02c	3.8435	3.8431	0.013%
0.04c	3.6929	3.6923	0.016%
-0.02c	4.1637	4.1633	0.010%
-0.04c	4.3338	4.3333	0.012%

can be conducted through the examination of the echo spectrum. Table 3 presents the numerical and theoretical results (26) of the frequency of the scattered field for a high-speed target. The results indicate that the relative error between the two outcomes falls within an acceptable range. This finding further supports the accuracy and validity of the proposed method:

$$\omega_s = \gamma\omega' \left(1 - \beta \frac{\cos\theta + \beta}{1 + \beta\cos\theta}\right). \tag{26}$$

V. CONCLUSION

In this paper, the EM model of a moving dispersive medium is established by utilizing the relativistic principle. In this study, we aim to investigate the scattering properties of high-speed moving plasma coated targets and their interaction with EM waves. To achieve this, we present and analyze two cases in order to reveal the nature of this work.

The first research example reveals that scattering and echo characteristics of the object exhibit a significant dependence on the velocity of the target, the direction of its motion, and the shape of the object. The second example examines the impact of plasma parameters, incidence direction, frequency of electromagnetic waves, and object velocity on the scattered field. The research findings indicate that the relative dielectric coefficient of the plasma sheath undergoes changes as a result of the object's velocity, thereby influencing the scattering and absorption of electromagnetic waves by the plasma. Additionally, the RCS exhibits distinct variations in pattern with target velocities when subjected to EM waves at different operating frequencies.

In future research, the Lorentz-FDTD algorithm will be applied to investigate and analyze more-complex EM scattering scenarios, such as considering the flow field properties of plasma sheaths and investigating the effect of spatial-temporal non-uniformity of plasma on EM imaging of high-speed moving object.

ACKNOWLEDGMENT

This work was supported by the National Natural Science Foundation of China (Nos. 62071003, 62201001), the Key Basic Research Project of the State Administration of Science, Technology and Industry for National Defense, China, the Open Project of the Key Laboratory of Computational Intelligence and Signal Processing, Ministry of Education (Grant No. 2020A008), the Natural Science Foundation of Education Department of Anhui Province, China (Grant No. KJ2020A0024), Anhui Provincial Natural Science Foundation (No. 2208085QF184), the Open Research Fund of Advanced Laser Technology Laboratory of Anhui Province, China (No. AHL2020KF04), the Open Project of the State Key Laboratory of Millimeter Waves (Grant No. K202222).

The authors are with the Information Materials and Intelligent Sensing Laboratory of Anhui Province, Anhui University, Hefei 230601, China, and also with the Anhui province Key Laboratory of Target Recognition and Feature Extraction, Luan 237000, China (The corresponding author is Yong Bo, email: boyong@ahu.edu.cn).

REFERENCES

[1] J. P. Rybak and R. J. Churchill, "Progress in reentry communications," *IEEE Transactions on Aerospace and Electronic Systems*, AES-7, NO.5:879-894, 1971.

[2] K. Lemmer, *Use of a Helicon Source for Development of a Re-entry Blackout Amelioration System*, 1-23, Michigan: University of Michigan, 2014.

[3] T. C. Lin and L. K. Sproul, "Influence of reentry turbulent plasma fluctuation on EM wave propagation," *Comput. Fluids*, vol. 35, no. 7, pp. 703-711, Aug. 2006.

[4] M. Kundrapu, J. Loverich, K. Beckwith, P. Stoltz, A. Shashurin, M. Keidar, and A. Ketsdever, "Modeling radio communication blackout and blackout mitigation in hypersonic vehicles," *J. Spacecr. Rockets*, vol. 52, no. 853, pp. 2-27, 2015.

[5] L. Shi, B. L. Guo, Y. M. Liu, and J. T. Li, "Characteristics of plasma sheath channel and its effect on communication," *Progress in Electromagnetic Research*, vol. 123, no. 2, pp. 321-336, 2012.

[6] C. T. Swift, F. B. Beck, J. Thomson, and S. L. Castellow, "RAM C-III S-band diagnostic experiment," in *Proc. NASA SP-252 4th Plasma Sheath Symp,* Washington, DC, USA, pp. 137-155, Jan. 1971.

[7] M. Chung and S. S, "FDTD simulations on radar cross sections of metal cone and plasma covered metal cone," *Vacuum: Technology Applications & Ion Physics: The International Journal & Abstracting Service for Vacuum Science & Technology*, vol. 86, no. 7, pp. 970-984, 2012.

[8] B. T. Nguyen, A. Samimi, and J. J. Simpson, "Recent advances in FDTD modeling of electromagnetic wave propagation in the iono-

sphere," *Applied Computational Electromagnetics Society (ACES) Journal*, vol. 29, no. 12, pp. 1003-1012, 2014.

[9] M. Pourbagher and S. A. Sahafi, "Three dimensional FDTD algorithm for wave propagation in cold plasma media using Forth-Order schemes," *Applied Computational Electromagnetics Society (ACES) Journal*, vol. 28, no. 12, pp. 1153-1161, 2013.

[10] K. S. Zheng, J. Z. Li, G. Wei, and J. D. Xu, "Analysis of Doppler effect of moving conducting surfaces with Lorentz-FDTD method," *Journal of Electromagnetic Waves and Applications*, vol. 27, no. 2, pp. 149-159, Feb. 2013.

[11] K. S. Zheng, X. P. Liu, Z. Mu, and W. Gao. "Analysis of scattering fields form moving multilayered dielectric slab illuminated by an impulse source," *IEEE Antennas Wireless Propag. Lett*, vol. 16, pp. 2130-2134, Jul. 2017.

[12] Y. Zhao and S. Chaimool, "Relativistic finite-difference time-domain analysis of high-speed moving metamaterials," *Scientific Reports*, vol. 8, no. 1, pp. 7686, 2017.

[13] T. J. Garner, A. Lakhtakia, J. K. Breakall, and C. F. Bohren, "Lorentz invariance of absorption and extinction cross sections of a uniformly moving object," *Physical Review A*, vol. 96, no. 5, pp. 053839, 2017,

[14] T. J. Garner, C. F. Bohren, A. Lakhtakia, and J. K. Breakall, "Electromagnetic pulse scattering by a spacecraft nearing light speed," *Applied Optics*, vol. 56, no. 22, pp. 6206-6213, 2017,

[15] G. Z. Niu, Y. M. Liu, B. W. Bai, and D. Yi, "A numerical simulation method of radar echo from a high-speed target," *IEEE Antennas Wireless Propag. Lett*, vol. 20, no. 10, pp. 1958-1962, Aug. 2021.

[16] L. Man, H. C. Deng, Y. Bo, Z. H. Xiao, and L.X. Yang, "Interaction between relative moving plasma plate and electromagnetic wave," *Chinese Journal of Radio Science*, vol. 38, no. 1, pp. 164-172, May 2022.

[17] L. J. Guo and L. X. Guo, "Absorption of electromagnetic waves by a moving non-uniform plasma," *Physics of Plasmas*, vol. 24, no.4, pp. 042119, 2017.

[18] Z. Bian, J. T. Li, L. X. Guo, and X. Luo, "Analyzing the electromagnetic scattering characteristics of a hypersonic vehicle based on the inhomogeneity zonal medium model," *IEEE Transactions on Antennas and Propagation*, vol. 69, no. 2, pp. 971-982, 2021.

[19] X. M. Guo, Y. Bo, L. X. Yang, M. P. Jin, Z. X. Huang, and H. Y. Li, "Study on Scattering Properties of Moving Cone-Sphere Shape Coated with Plasma Sheath," *2022 IEEE 5th International Conference on Electronic Information and Communication Technology*, pp. 775-778, 2022.

[20] H. W. Yang, R. S. Chen, and Y. Zhang, "SO-FDTD method and its application to the calculation of electromagnetic wave reflection coefficients of plasma," *Chinese Physics*, vol. 55, no. 7, pp. 3464-3469, 2006.

[21] Z. K. Zhou, X. H. Wan. X. L. Li, J. Zhang, Y. S. Zhou, X. P. Ren, and Y. R. Shi, "SO-FDTD analysis on transmission characteristics of terahertz wave in plasma," *Physics of Plasmas*, vol. 28, no. 7, pp. 1-8, 2021.

[22] C. Wei, L. X. Yang, Z. X. Huang, and L. X Guo, "Research on the propagation characteristics of THz waves in spatial inhomogeneous and time-varying and weakly ionized dusty plasma," *IEEE Trans. Plasma Sci*, vol. 47, no. 10, pp. 4745-4752, Oct. 2019.

[23] K. S. Zheng, Y. Li, L. Xu, J. T. Li, and G. Wei, "Electromagnetic properties of a complex pyramid-shaped target moving at high speed," *IEEE Trans. Antennas Propag*, vol. 66, no. 12, pp. 7472-7476, Dec. 2018.

[24] Jinau Kong, *Electromagnetic Waves Theory* 2, *Higher Education Press*, 2000.

[25] D. B. Ge and Y. B. Yan, *The Finite-Difference Time-Domain Method for Electromagnetic Wave*, 151-155. Xi'an, China: Xidian Univ. Press, 2011.

[26] Y. G. Lv, L. X. Guo, and J. T. Li, *Hypersonic Vehicle Plasma Sheath and Electromagnetic Characteristics Data Manual*, Beijing, China: Science Press, 2019.

[27] Z. W. Liu, W. M. Bao, X. P. Li, and D. L. Liu, "A segmentation calculation method for plasma collision frequency considering the electromagnetic wave driving effect," *Acta Phys. Sinica*, vol. 63, no. 23, 2014,

Xian-Min Guo was born in Xianyang City, Shanxi Province, China, in 1999. She received the B.S. degree in electronic information engineering from Shandong University of Technology, Zibo, China, in 2021. She is currently working toward the master's degree in electromagnetic field and microwave technology of Electronic Information with the School of Electronic Information Engineering, Anhui University, Hefei, China.

Her current research interest is computational electromagnetism and plasma physics.

Hai-Yan Li was born in Huaibei City, Anhui Province, China, in 1999. She received the B.S. degree in electronic information engineering from Huainan Normal University, Huainan, China, in 2021. She is currently working toward the master's degree in electromagnetic field and microwave technology of Electronic Information with the School of Electronic Information Engineering, Anhui University, Hefei, China.

Her current research interest is computational electromagnetism.

Yong Bo was born in Shandong Province, China, on November 11, 1989. He received the B.S. degree in Shandong University of Science and Technology, Qingdao, China, in 2012, and the Ph.D. degree from the Center for Information Geoscience, University of Electronic Science and Technology of China, Chengdu, China.

He is currently a lecturer with the University of Anhui, Hefei, China. The main subjects of his interest include computational electromagnetic, wave propagation in plasmas, and low temperature plasma technology and application.

Wei Chen was born in Jiangsu Province, China, in 1987. He received the B.S. and M.S. degrees from Jiangsu University, Jiangsu, China, in 2010 and 2013, respectively, and the Ph.D. degree from Xidian University, Xi'an, China, in 2018.

He is currently a lecturer with the School of Electronics and Information Engineering, Anhui University, Hefei, China. His current research interests include numerical methods in electromagnetic scattering from plasma and wave propagation in complex systems.

Li-Xia Yang was born in Ezhou, Hubei, China, in 1975. He received the B.S. degree in physics from Hubei University, Wuhan, China, in 1997, and the Ph.D. degree in radio physics from Xidian University, Xi'an, China, in 2007.

Since 2010, he has been an associate professor with the Communication Engineering Department, Jiangsu University, Zhenjiang, China. From 2010 to 2011, he was a postdoctoral research fellow with the Electro Science Laboratory (ESL), Ohio State University, Columbus, OH, USA. From 2015 to 2016, he was a visiting scholar with the Institute of Space Science, University of Texas at Dallas, Dallas, TX, USA. From 2016 to 2019, he was a professor, a Ph.D. supervisor, and the chairman of the Communication Engineering Department, Jiangsu University. Since 2020, he has been a distinguished professor, a Ph.D. supervisor, and the vice dean with the School of Electronic and Information Engineering, Anhui University, Hefei, China. His research interests include wireless communication technique, radio sciences, computational electromagnetics, and the antenna theory and design in wireless communication systems. He is a member of the Editorial Board of Radio Science Journal in China.

Zhi-Xiang Huang was born in Anhui, China, in 1979. He received the B.S. and Ph.D. degrees from Anhui University, Hefei, China, in 2002 and 2007, respectively. He was a visiting scholar with Iowa State University, USA, from September 2010 to September 2011. From August 2013 to October 2013, he was a visiting professor with The University of Hong Kong. From February 2014 to February 2015, he was a visiting professor with the Beijing National Laboratory for Condensed Matter Physics, Institute of Physics, Chinese Academy of Sciences. He has published one monograph on the symplectic finite-difference time-domain method and two book chapters at CRC Press and In Tech Publishers. He has published 60 peer-reviewed journal articles included in the Web of Science Core Collection. His current research interests include time-domain numerical methods, metamaterials, and active metamaterials. He is a member of the OSA. In 2015, he was awarded the second prize of Science and Technology from the Anhui Province Government, China, and the National Science Foundation for Outstanding Young Scholar of China, in 2017.

An-Qi Wang was born in Anhui, China, in 1986. She received the B.S. and Ph.D. degrees from Xidian University, Xi'an, China, in 2007 and 2013, respectively. Her current research interests include computational electromagnetics and the electromagnetic wave scattering characteristics of rough surface and targets.